General Disclaimer

One or more of the Following Statements may affect this Document

- This document has been reproduced from the best copy furnished by the organizational source. It is being released in the interest of making available as much information as possible.

- This document may contain data, which exceeds the sheet parameters. It was furnished in this condition by the organizational source and is the best copy available.

- This document may contain tone-on-tone or color graphs, charts and/or pictures, which have been reproduced in black and white.

- This document is paginated as submitted by the original source.

- Portions of this document are not fully legible due to the historical nature of some of the material. However, it is the best reproduction available from the original submission.

NASA TECHNICAL MEMORANDUM

NASA TM-73877

NASA TM-73877

HIGH TEMPERATURE SURFACE PROTECTION

by Stanley R. Levine
Propulsion Laboratory
U.S. Army R&T Laboratories (AVRADCOM)
NASA Lewis Research Center
Cleveland, Ohio 44135

TECHNICAL PAPER to be presented at the
Spring Review Conference of the
Institution of Metallurgists
Cardiff, Wales, April 7-10, 1978

HIGH TEMPERATURE SURFACE PROTECTION

Stanley R. Levine
Propulsion Laboratory, US Army R&T Laboratories, NASA-Lewis Research Center, Cleveland, Ohio

Alloys of the MCrAlX type are the basis for high temperature surface protection systems in gas turbines. M can be one or more of Ni, Co, or Fe and X denotes a reactive metal added to enhance oxide scale adherence. The selection and formation as well as the oxidation, hot corrosion and thermal fatigue performance of MCrAlX coatings are discussed. Coatings covered range from simple aluminides formed by pack cementation to the more advanced physical vapor deposition overlay coatings and developmental plasma spray deposited thermal barrier coatings.

INTRODUCTION

The field of high temperature surface protection is very broad. However, there are many similarities in both performance requirements and approaches to achieve such protection for a wide variety of applications. Consequently, this survey focuses on only one application which represents many others --- the surface protection of the hot section components of gas turbine engines. Even with this restricted scope, it is not my intent to exhaustively cover the field. This has already been done in reviews by Grisaffe (1), Chatterji, et al (2) and the Committee on Coatings of the National Materials Advisory Board (3).

In gas turbines, primary concern centers on protection of nickel- and cobalt-base alloys from environmental degradation by four interactive processes: oxidation, erosion caused by particulates, hot corrosion from air or fuel derived impurities and thermal fatigue resulting from cyclic thermal stresses. The object of surface protection is to retard these processes while causing no strength or ductility degrading reactions with the alloys. Gas turbine protection problems, principles and methods provide the framework for this paper and the work of my colleagues at the NASA Lewis Research Center and work conducted under NASA funding will provide most of the illustrative material.

HIGH TEMPERATURE PROTECTION MECHANISM

The key to the use of metallic materials in a thermodynamically agressive environment is control of the reaction kinetics so that useful, economic lifetimes are obtained. The preferred method for doing this is to design or select an alloy which slowly forms a dense, adherent and stable reaction product. With nickel- and cobalt-base gas turbine alloys the available protective oxide formers are the base metals and chromium or aluminum. As can be seen from Table I, the preferred oxides are chromia and alumina. Because of the performance benefits derived from high turbine inlet temperatures, alloy environmental resistance, and hot corrosion resistance in particular, is often sacrificed for high-temperature strength in nickel-base alloys. This is generally accomplished by reduction of chromium content and increases in refractory metal content (5). In the absence of sufficiently resistant alloys, control of reaction kinetics falls upon protective coatings.

Coatings are generally an add-on "fix" rather than an integral part of system design. The object with metallic coatings is to provide a layer rich in Cr and/or Al so that the preferred protective oxides can again form. Since metallic coatings are generally applied 0.008 to 0.013 cm thick, their protective capability is limited by the kinetics of protective element consumption by reaction with the environment, spalling or erosion of the protective oxide scale and interdiffusion with the substrate. High-temperature metallic coatings for superalloys are based on three ternary systems: Ni-Cr-Al, Fe-Cr-Al and Co-Cr-Al. Depending on the particular chemistry selected, these alloys can form the base-metal oxide, Cr_2O_3, Al_2O_3, mixed oxides or spinels. This is illustrated

TABLE 1 - Parabolic Growth Rate Constants for Gas Turbine Alloy Oxide Scales (4).

Temperature, ^{o}C	kp (g^2/cm^4 - sec)			
	CoO	NiO	Cr_2O_3	Al_2O_3
1000	$1.2x10^{-8}$	$7.5x10^{-11}$	$2.3x10^{-11}$	$9.0x10^{-14}$
1100	$2.5x10^{-8}$	$2.2x10^{-10}$	$9.0x10^{-11}$	$6.5x10^{-13}$

in Figure 1 by the 1100 to 1200^{o}C oxide map of cyclic oxidation in the Ni-Cr-Al system (6). In all three systems, as illustrated by the boundary of region I in the figure, the addition of chromium reduces the amount of aluminum required for Al_2O_3 formation. A combination of thermodynamic and kinetic factors are responsible for this phenomenon (4). A second phenomenon common to all three systems is the large improvement in cyclic oxidation resistance obtained by addition of small quantities of noble or reactive metals such as Pt, Zr, Y and Si (typically less than 1 wt %) and by additions of finely dispersed oxides such as ThO_2, Y_2O_3 and ZrO_2 (typically 2 wt %) (4). A number of theories on the mechanism of improved scale adherence by each class of additive can be found in the literature. Regardless of the mechanism, these phenomena are important for the coating designer to take advantage of. A useful guide for the coating or alloy developer is the corrosion map delineating either the oxide scales formed, as shown previously, or corrosion resistance. An example of an oxidation map is shown in Figure 2 (6). This map indicates the cyclic oxidation resistance of Ni-Cr-Al alloys containing about 0.5 w/o of the reactive element as zirconium or zirconium oxide. Combining this information with similar maps for hot corrosion of Ni-Cr-Al alloys indicates that in still air tests an optimum balance of oxidation and hot corrosion resistance is obtained at about Ni-30 w/o Cr-10 w/o Al (7).

Metallic coatings for gas turbine alloys fall into two basic generic classes based on formation mechanism. The first class consists of aluminide coatings. At some point in their formation a diffusion reaction with the substrate surface occurs to form the major coating phase, β-NiAl. With reference to Figure 2, these coatings generally fall in the region of good oxidation resistance extending from the apex of the diagram. The most common method of forming aluminide coatings is the pack cementation process wherein aluminum bearing vapor species react with the substrate at elevated temperature to deposit aluminum and form Ni_2Al_3 or NiAl (8). Other methods include metallizing, chemical vapor deposition, slurry fusion and hot dipping. The pack cementation process places severe restrictions on the coating chemistries available by a one-step process. For example, it is not possible to achieve the better NiCrAl coating compositions by a simple aluminizing process. Many attempts to circumvent this limitation have been made. The major approach has been to first deposit a modifier layer by pack cementation, electroplating, slurry spraying (9, 10), cladding (11), plasma spraying, etc., and then perform the aluminizing step. This approach is based on (1) exclusion of undesirable refractory metal substrate elements from the coating and (2) improvement of ductility, hot corrosion and/or oxidation resistance by adding one or more desirable modifier elements and, in many cases, moving toward the second generic coating class - metallic overlays.

As their class name suggests, overlays are add-on coatings which do not depend on a diffusion reaction with the substrate for formation or composition (although some diffusion is necessary to form a sound metallurgical bond). Available techniques include physical vapor deposition (12), sputtering, slurry fusion, plasma spraying (13) and cladding (11). Here compositional flexibility is virtually unlimited. However, achievement of a proper balance between ductility, oxidation resistance and hot corrosion resistance often enforces composition limitations. For example, in the NiCrAl system, Figure 2, we are generally restricted to the central region of the diagram when coating ductility is an overriding factor. In this region of improved ductility, the primary coating phases are β-NiAl and γ-Ni solid solution.

The MCrAlY overlay coatings deposited by plasma spraying are also used as a component in a second coating method for protecting air cooled turbine components - thermal barrier coatings (13, 14, 15). The protection principle here is to reduce the component metal temperature by placing an insulating coating on the outer airfoil surface. The insulating coating is usually stabilized ZrO_2 which is plasma spray deposited over the MCrAlY bond coat. The bond coat gives oxidation protection to the substrate and improves adhesion of the ceramic. The bond coat is typically applied 0.013 cm thick and the insulating layer can be applied 0.025 to 0.050 cm thick.

With this background in surface protection principles and methods behind us, three coatings -- pack aluminides, overlays and thermal barriers can now be treated in more detail.

PACK ALUMINIDE COATINGS

Formation

In the pack cementation process the parts to be coated are supported in a coating pack. The pack contains an aluminum source typically as aluminum or a prealloyed aluminum-containing alloy and a halide "activator" such as AlF_3, $CrCl_3$, NH_4Cl, NaF, etc. If the source or activator are prone to sintering or fusing to the substrate an inert filler such as Al_2O_3 is used to dilute the pack. The pack is heated in a sealed or open retort at ambient pressure or under vacuum so that aluminum is transported via the gas phase to the part surface where it reacts to form an aluminide coating.

The work of Goward and Boone (8) and analytical treatments by Walsh (16), Levine and Caves (17), Seigle and co-workers (18-21) and Hickl and Heckel (22) have recently provided a good understanding of the pack aluminizing process. Goward and Boone (8) provided a foundation for the later analytical treatments by determining the diffusion mechanisms and coating structures obtained at the practical processing extremes. At high temperatures (>1000°C) in packs with aluminum sources having a limited capability to supply aluminum, β-NiAl coatings are formed by outward diffusion of nickel (Figure 3a). The aluminum supply is limited either because the source is prealloyed (Goward and Boone's "low activity pack") or because the pack is dilute (17). On a superalloy, the dominant coating feature is an outer large-grained, single-phase NiAl layer having a relatively low content of substrate alloying elements. The diffusion zone contains columnar NiAl and/or Ni_3Al, carbides and, in some cases, σ. At lower temperatures (<1000°C) in packs having more potent aluminum sources (Goward and Boone's "high activity packs") the surface phase is primarily Ni_2Al_3 formed by inward aluminum diffusion (Figure 3b). Because the reaction occurs by inward diffusion, on superalloys these coatings contain relatively high concentrations of substrate alloying elements and incorporated carbides. Inner layers of the coating consist of Ni_2Al_3 and NiAl followed by NiAl. Ni_2Al_3 is a brittle, relatively low melting phase. These coatings are converted to β-NiAl by a diffusion anneal (Figure 3c). Inward aluminum diffusion continues until the β layer becomes Ni-rich. Then Ni diffuses outward through NiAl while inward Al diffusion continues in Ni_2Al_3 and Al-rich β until they are consumed. The result is a coating with an outer fine-grained NiAl layer containing α-(Cr, Mo) precipitates and carbides, an essentially single-phase, coarse-grained intermediate layer containing substrate elements in solution and a columnar diffusion zone consisting primarily of β, carbides and σ.

From the preceding discussion it is apparent that the aluminizing process is a complex phenomenon involving thermodynamics and kinetics of reactions in the gaseous and solid states. Since the steps occur in series, the process is self-regulating in the sense that driving forces for each step adjust so that all steps proceed at the same rate. Because of the complexity of dealing with the solid-state problem when the substrate is a multi-element, multi-phase superalloy, the Levine and Caves treatment of high temperature aluminizing from packs containing a dilute pure aluminum source was confined to the gas phase by assuming a coating surface aluminum activity of 10^{-2} (17). The key to this problem was recognition of the fact that a depleted zone is formed in the pack as illustrated in Figure 4. A mass balance equating coating weight to aluminum removed from the pack depleted zone could then be applied. This resulted in a solution for the parabolic rate constant for the gas phase process:

$$k_g = \frac{2\rho\varepsilon}{\ell RT} \sum_{i=1}^{n} D_i \, (P_i - P_i') \times 2.7 \times 10^4 \qquad (1)$$

Here ρ is the pack Al concentration in mg/cm^3, ε is the pack porosity, ℓ is a correction factor for diffusion of a gas in a porous medium, RT has the conventional meaning, D_i is the diffusion coefficient of the i^{th} Al bearing species and P_i and P_i' are the partial pressures of the i^{th} species in the bulk pack and at the coating/pack interface as determined from thermodynamic and kinetic considerations. This analysis resulted in a potency ranking of activators (F>Cl>Br>I) in agreement with experimental observations.

A more exact treatment of the problem is possible if the substrate is pure nickel, as in the NASA-funded work by Seigle and co-workers. They established that coating surface composition rapidly reaches a steady state value for a given set of pack conditions (18). This permitted them to tackle the simultaneous solution of the solid-state (19) and gaseous diffusion problem with no a priori assumption about coating surface composition (17). Surface composition is defined by the point at which

$$k_s = k_g \qquad (2)$$

Here k_s is the parabolic rate constant for the solid-state part of the formation process. Some results are shown in Figure 5 for a 4w/oAlF$_3$ activated, 4w/o aluminum pack. Agreement between the theoretical predictions and experimental results are excellent at 800°C. At 1093°C larger

discrepancies were reported (20). Two possible causes for these discrepancies are: (1) reduction of the deposition rate by condensation of AlF_3 in pack pores and (2) losses of Al from the pack. The k_g curves for activators such as NaF, NaCl and NaI are similar in shape to the one shown for AlF_3, but the rate constants are smaller (21).

The pack depleted zone model illustrated in Figure 4 can be modified to a linear depleted zone concentration profile in the case of alloyed packs. Then the approach of Levine and Caves (17) can be applied to obtain a family of k_g curves for each activator as a function of source aluminum content. The intersections of these curves with the k_g curves gives the surface composition and rate of coating formation.

Performance

The Mach I burner rig performance of a simple aluminide coating and duplex Pt and NiCrAl modified coatings on cast wedge bar specimens of IN-100 and NASA TRW VIA nickel-base superalloys are compared in Table 2 (23, 24). All three coatings offer improved oxidation and thermal fatigue resistance with the NASA developed duplex coating offering the largest gains. In all three cases, better coating performance is obtained with the VIA substrate. An example of the effect of temperature on coating visual failure life in the Mach I burner rig is shown in Figure 6 for aluminized WI-52 (25). A 55°C increase in temperature decreased coating life by a factor of five.

TABLE 2 - Coating Life in Mach I Burner Rig (23, 24)

Cycle: 1 hour at 1093°C, 5 minutes cool to room temperature

Substrate	IN-100		NASA TRW VI-A	
Coating	Cycles to First Weight Loss	Cycles to Thermal Fatigue Crack	Cycles to First Weight Loss	Cycles to Thermal Fatigue Crack
None	<20	40	<20	40
Pack Aluminide	180	160	220	200
Pt + Aluminide	720	420	1100	420
NASA NiCrAl + Aluminide	800	520	1120	680

The results of 900°C, Mach 0.3 burner rig hot corrosion are given in Table 3 for two aluminide coatings on three Ni-base superalloy substrates (26). Both coatings were formed in low activity packs. Coating A had deliberate α-Al_2O_3 inclusions. Coating life correlated fairly well with coating thickness regardless of the coating or substrate (26).

The mechanical effects of aluminide coatings are well documented in the literature. The bulk of the work has been performed on relatively large gage section specimens. Here, no significant effect on stress-rupture life or tensile properties is seen since the coated area is small in relation to specimen cross-sectional area. The work of Kaufman (27) is an exception. He examined the effect of a Codep aluminide coating on thin cast Rene' 80 and Rene' 120. In stress-rupture the effect of section thickness was larger than the effect of coating at temperatures from 760 to 1093°C. The coating decreased the life of thin sections (0.038 to 0.15 cm) when stresses were calculated on the basis of bare specimen dimensions. Stress-rupture life was reduced by the coating only at 760°C if calculated on the basis of sound unaffected metal. In another study Anderson, et al (28) observed a difference in the effect of the two generic aluminide coating classes on the fatigue behavior of Ni-base superalloys. In room temperature to 1900°F thermal fatigue and 1400°F high-cycle fatigue an inwardly grown aluminide coating was superior to an outwardly grown coating on U-700 and B-1900. They attributed this difference to the superior strength and ductility of the fine-grained surface layer of the inwardly grown coating.

TABLE 3 - Failure Times of Coated Alloys in Burner Rig Hot Corrosion (26).

900°C, Mach 0.3, 5 ppm sea salt				
	Time to Failure+ hours (cycles)		Specific Time to Failure* hours per micron of coating	
Specimen	Ten Minute Cycles	One Hour Cycles	Ten Minute Cycles	One Hour Cycles
IN-713C				
Coating A	65 (390)	60 (60)	0.75	0.6
Coating B	50 (300)	70 (70)	0.60	0.8
IN-100				
Coating A	40 (240)	30 (30)	0.55	0.3
Coating B	42.5 (255)	55 (55)	0.65	0.7
B-1900				
Coating A	55 (330)	55 (55)	0.65	0.6
Coating B	40 (240)	45 (45)	0.65	0.9

+Failure criterion: 50 mil diameter pit penetrating to the substrate
*Time to failure divided by the initial coating thickness

Degradation

There has been considerable controversy over whether oxidation or interdiffusion is the primary cause of aluminide coating degradation in an oxidizing environment. This issue was recently clarified by Smialek and Lowell (29). Figure 7 shows their as-deposited aluminide coating on Ni-base superalloy Mar-M-200. This microstructure indicates coating formation in a "low-activity pack." After a diffusion anneal at 1100°C for 300 hours in an inert environment the coating approximately doubled in thickness as can be seen in Figure 8. Electron microprobe traces for aluminum, Figure 9, indicate a substantial reduction in concentration from the as-coated level. Cyclic oxidation for 700 hours at 1100°C did not result in an aluminum concentration profile appreciably different from the profile resulting from the 300 hour anneal. Based on these profiles and the fact that the 300 hour diffusion anneal reduced coating life by nearly 300 hours, the authors concluded that interdiffusion is the triggering mechanism for rapid coating degradation. Diffusion causes dilution of the coating which permits formation of oxides less protective than Al_2O_3. This leads to rapid coating failure due to the increased rate of oxide spalling.

OVERLAY COATINGS

The equipment required to deposit overlay coatings by physical vapor deposition (PVD), sputtering (SD), or plasma spraying is far more complex than that used in pack aluminizing. In the PVD process the coating is formed by evaporation of atoms from one or more electron beam melted elemental or alloy sources. In sputtering, atoms from the source are ejected by collisions with an ionized inert gas. The gas is generated by collisions with electrons emitted by the source. In the plasma spray process particles of the coating material are gas transported through an arc where they are fused and propelled toward the substrate at high velocity. The major problem with all three methods is control of the process so that coatings of uniform thickness and composition with a desirable microstructure are obtained. All three processes have some degree of line-of-sight limitation. PVD and SD formed deposits are prone to "leader" defects---oxide stringers or weakly bonded regions perpendicular to the substrate surface. Some solutions for leader defect and other PVD process problems have been discussed by Boone, et al (30). Plasma sprayed coatings tend to have a porous, shingled microstructure. Inert atmosphere spraying coupled with the new high energy equipment appears to be a potential solution to this problem.

Three factors have been responsible for the trend to overlay coatings: (1) The high ductile-to-brittle transition temperature (DBTT) of aluminide coatings, (2) the diffusional instability of aluminide coatings on higher temperature capability oxide dispersion strengthened alloys and directionally solidified eutectics and (3) hot corrosion.

According to Goward (31) the DBTT of aluminide coatings can range from about 650 to 750°C depending on aluminum content. With PVD coatings the DBTT can be adjusted over a range from 100°C

up to about 550°C by adjustment of aluminum content. Thus aluminide coatings can adversely affect fatigue life in thermal-mechanical fatigue cycles with stresses peaking at temperatures below the DBTT (31).

The need for overlay coatings on the directionally solidified eutectic γ/γ'-δ is illustrated by the data in Table 4 (32). Of the overlay coatings tested, the NiCrAlY+Pt variation was superior not only in furnace oxidation, but this coating also proved to be least prone to thermal fatigue cracking in burner rig tests. The ability to tailor overlay coatings to the substrate was illustrated in another coating development program for a directionally solidified eutectic (33). In this program it was found that PVD overlay coatings and the NASA duplex NiCrAl + aluminide (NASCOAT 70) coating caused reinforcing carbide fiber denudation of NiTaC-13. To overcome this loss of strengthening phase, NASCOAT 70 was carbon modified to Ni-20Cr-5Al-0.1C-0.1Y, deposited by plasma spraying and pack aluminized. This coating essentially eliminated the TaC fiber denudation problem.

TABLE 4 - Cyclic Furnace Oxidation Performance of γ/γ'-δ DS Eutectic (32)

1 hour cycles

Coating	Deposition Methods	Weight Change, mg/cm^2 500 hours, 1090°C	100 hours, 1205°C
None	----	-17.7 @ 40 hrs.	----
Aluminide	Pack	-1.25 @ 100 hrs.	----
CoNiCrAlY	PVD	+.42	Melting
NiCrAlY	PVD	+1.24	-4.5
NiCrAlY+Al	PVD + Pack	+.28	-2.6
NiCrAlY+Pt	PVD + Sputter	+.58	+.56

TABLE 5 - Cyclic Furnace Hot Corrosion Performance of γ/γ'-δ DS Eutectic (32)

870°C, 20-hour cycles, 260 hour test

	Deposition Methods	Total Weight Change, mg/cm$^{2(a)}$
None	----	4.9
Aluminide	Pack	1.5
CoNiCrAlY	PVD	.04
NiCrAlY	PVD	.15
NiCrAlY+Al	PVD + Pack	.40
NiCrAlY+Pt	PVD + Sputter	.07

(a) Specimens coated with 0.5 mg/cm^2 Na_2SO_4 every 20 hours.

The performance advantage of overlay coatings in hot corrosion is illustrated by the data in Table 5. Characteristically, the aluminide coating exhibited spot failures as did the PVD plus pack version of NiCrAlY + aluminide. The PVD coatings were intact at the end of the test.

The question of whether diffusion or oxidation is primarily responsible for overlay coating degradation has not been fully addressed. Overlay coatings are closer to superalloy compositions than are aluminides in terms of chromium and aluminum content. Also, the interdiffusion coefficient is considerably smaller with overlay coatings. Thus, it appears that interdiffusion should be less important in overlay coating degradation than in aluminide coating degradation (34). However, Gedwill (35, 36) has shown that at 1090°C substrate alloying elements such as Mo can rapidly diffuse from superalloys and degrade the oxidation resistance of cladding alloys.

THERMAL BARRIER COATINGS

Because their thermal conductivity is approximately 3% that of gas turbine alloys and their thermal expansion coefficient matches superalloys better than most other ceramics, stabilized zirconias can be used to form an effective thermal barrier on gas turbine airfoils as illustrated in Figure 10 (37). Thermal barrier coatings offer retrofit potential for existing engines or may be designed into new energy efficient engines. Preliminary analytical studies indicate that if the coating is used in a manner such that turbine inlet temperature is increased 80°C while cooling air flow is reduced 40 percent, the benefits with current blade and vane alloys are an 18 percent increase in thrust, a four-fold increase in part life, and a two percent decrease in fuel consumption. Alternatively, turbine inlet temperature may be increased over 150°C. This is equivalent to the growth in turbine inlet temperature achieved over the past decade through alloy improvements and turbine cooling.

In Figure 11, the microstructure of the as-plasma sprayed NASA duplex thermal barrier coating is shown (15). Since the coating was applied manually, there is about 0.005 cm of variation in thickness of the bond coat and oxide from location to location. This variation is evident for the bond coat layer in Figure 11. Both the bond coat and oxide are porous and display the characteristic shingled structure.

Coating development at NASA-Lewis is being carried out with the aid of furnace screening tests on solid coupon specimens. Better coatings are then tested in torches and Mach 0.3 and Mach 1 burner rigs. The results of cyclic furnace screening of various oxide thermal barrier layers are presented in Table 6 (15). The specimens were heated to 975°C in 4 minutes, held at temperature for 1 hour and cooled to 280°C in 1 hour. Of the oxides tested, yttria-stabilized zirconia

TABLE 6 - 975°C Cyclic Furnace Evaluation of Various Zirconia Thermal Barrier Coatings on Ni-16Cr-6Al-0.6Y Bond Coat (15)

Alloy	Cycles to failure[a] - First visible crack, spall, etc.			
	ZrO_2-12Y_2O_3	ZrO_2-3.4MgO	ZrO_2-5.4CaO-P[b]	ZrO_2-5.4CaO-T[c]
DS MAR-M-200 + Hf	[d]673	460	255	78
MAR-M-200 + Hf	[d]650	450	255	87
MAR-M-509	[d]558	450	196	76
B-1900 + Hf	[d]628	438	226	--

[a]Cycle, 1-hr at temperature and 1-hr to cool to 280°C.
[b]P, partially stabilized zirconia derived from ZrO_2 and $CaCO_3$ spray powders (cubic and monoclinic phases).
[c]T, totally stabilized zirconia derived from stabilized spray powder (cubic phase).
[d]No failure observed.

is clearly the best. This oxide was not previously as widely studied in the thermal barrier application as the other oxides listed due to its higher cost and lower availability.

In Mach 0.3 burner rig tests of cooled J-75 turbine blades, the ranking of the oxides was the same as in the furnace tests. The J-75 blades were heated nonuniformly and very severe local temperature gradients developed. Yttria stabilized zirconia survived as many as 3200 cycles consisting of 80 seconds at 1280°C surface temperature and a 915°C substrate temperature followed by cooling to 75°C. The yttria stabilized zirconia coating also survived 182 cycles consisting of 1 hour at a 1425°C surface temperature and 925°C substrate temperature followed by cooling to 75°C. Both tests were terminated due to erosion of the coating to about half its initial thickness (15). This erosion, attributed to carbon from the Jet A fueled burner, is of considerable concern. In tests carried out in a natural gas fired Mach 1 burner rig, erosion was not evident.

The NiCrAlY bond coat in conjunction with calcia, magnesia, and yttria stabilized zirconia thermal barriers were run on first stage turbine blades in a J-75 research engine. After 500 2-minute cycles between full power and engine flameout all coated blades were in good condition (14). At full power engine conditions were: 1370°C turbine inlet temperature, 3 atm and 8300 rpm. At flameout the conditions were: 730°C, 1 atm and 3300 rpm. Coating surface temperature was as high as 1080°C, blade metal temperature was as high as 930°C and the temperature drop through the coating was as high as 135°C at full power. At flameout the blade metal temperature was 530°C.

Presently efforts are underway to improve the coatings and develop the technology needed to place them in gas turbines. The primary problem is to develop tolerance to the cyclic thermal-mechanical stress environment. This will require a new integrated design approach where the coating and airfoil are considered as a system throughout the design process.

CONCLUDING REMARKS

In a review such as this it is possible to do no more than touch on highlights of a subject as broad as high temperature surface protection. If I have succeeded in acquainting you with high temperature gas turbine surface protection principles and methods, my purpose has been accomplished. For those closer to the field, I have tried to include state-of-the-art material and to expose some of the gaps in the technology.

We are now entering a new era in this field. Declining fossil fuel reserves present us with many challenging problems. We must have our engines run more efficiently by operating at higher temperatures, use less desirable fuels and yet achieve longer lives to conserve mineral resources as well. These needs span aircraft and stationary gas turbines. Protective coatings have great potential for helping us solve some of these problems. Realization of this potential will not be an easy task.

REFERENCES

1. Grisaffe, S.J., 1972, "Coatings and Protection", p. 341, "The Superalloys", Sims, C.T., and Hagel, W.C., Eds., John Wiley and Sons, Inc., New York.

2. Chatterji, D., et al, 1976 "Protection of Superalloys for Turbine Application", p. 1, "Advances in Corrosion Science and Technology 6", Fontana, M.G., and Staehle, R.W., Eds., Plenum Press, New York.

3. Committee on Coatings, National Materials Advisory Board, 1970, "High Temperature Oxidation-Resistant Coatings", National Academy of Sciences, Washington, D.C.

4. Pettit, F.S., et al, 1976, "Oxidation and Hot Corrosion Resistance", p. 349, "Alloy and Microstructural Design", Tien, J.K. and Ansell, G.S., Eds., Academic Press, Inc., New York.

5. Freche, J.C., 1976, "Stress Rupture Resistance", p. 145, ibid.

6. Barrett, C.A. and Lowell, C.E., 1976, "Resistance of Nickel-Chromium-Aluminum Alloys to Cyclic Oxidation at 1100°C and 1200°C", NASA TN D-8255.

7. Santoro, G.J. and Barrett, C.A., 1977, "Hot Corrosion Resistance of Nickel-Chromium-Aluminum Alloys", NASA TM X-73664.

8. Goward, G.W. and Boone, D.H., 1971, Oxidation of Metals 3, 475.

9. Smialek, J.L., 1971, "Exploratory Study of Oxidation-Resistant Aluminized Slurry Coatings for IN-100 and WI-52 Superalloys", NASA TN D-6329.

10. Stevens, W.G. and Stetson, A.R., 1976, "Controlled Composition Reaction Sintering Process for Production of MCrAlY Coatings", AFML-TR-76-91.

11. Gedwill, M.A. and Grisaffe, S.J. 972, Metals Engineering Quarterly 12, 55. Also 1975, "Duplex Aluminized Coatings", U.S. Patent 3, 869, 779.

12. Talboom, F.P., et al, 1970, "Evaluation of Advanced Superalloy Protection Systems", NASA CR-72813.

13. Tucker, R.C., et al, 1976, "Plasma Deposited MCrAlY Airfoil and Zirconia/MCrAlY Thermal Barrier Coatings", Union Carbide Corporation, Indianapolis, Ind.

14. Liebert, C.H., et al, 1976, "Durability of Zirconia Thermal-Barrier Ceramic Coatings on Air-Cooled Turbine Blades in Cyclic Jet Engine Operation", NASA TMX-3410.

15. Stecura, S., 1976, "Two-Layer Thermal Barrier Coating for Turbine Airfoils - Furnace and Burner Rig Test Results", NASA TMX-3425.

16. Walsh, P.N., 1973, "Chemical Aspects of Pack Cementation", p. 147, "Chemical Vapor Deposition", Wakefield, G.F. and Blocher, J.M., Eds., The Electrochemical Society, Princeton, New Jersey.

17. Levine, S.R. and Caves, R.M., 1974, Journal of the Electrochemical Society 121, 1051.

18. Sivakumar, R., et al, 1973, Metallurgical Transactions 4, 396.

19. Sarkhel, A.K. and Seigle, L.L., 1976, Metallurgical Transactions 7A, 899.

20. Sivakumar, R. and Seigle, L.L., 1976, Metallurgical Transactions 7A, 1073.

21. Gupta, B.K., et al, 1976, Thin Solid Films 39, 313.

22. Hickl, A.J. and Heckel, R.W., 1975, Metallurgical Transactions 6A, 431.

23. Deadmore, D.L., 1972 "Cyclic Oxidation of Cobalt-Chromium-Aluminum-Yttrium and Aluminide Coatings on IN-100 and VIA Alloys in High-Velocity Gases", NASA TN D-6842.

24. Lowell, C.E., et al, 1975, "Environmental Effects and Surface Protection of High Temperature Alloys: A Review of NASA-Lewis Programs", MCIC Report 75-27, "Proceedings of 1974 Gas Turbine Materials in the Marine Environment Conference", Castine, Maine, p. 535.

25. Grisaffe, S.J., et al, 1970 "Furnace and High-Velocity Oxidation of Aluminide-Coated Cobalt Superalloy WI-52", NASA TN D-5834.

26. Santoro, G., 1975 "Hot Corrosion Evaluation of Aluminide Coated Superalloys in Support of an ASTM Round Robin Program", NASA TMX-71734.

27. Kaufman, M., 1974, "Examination of the Influence of Coatings on Thin Superalloy Sections, Volume I - Description and Analysis", NASA CR-134791.

28. Anderson, P.J., et al, 1972, Oxidation of Metals 4, 113.

29. Smialek, J.L. and Lowell, C.E., 1974, Journal of the Electrochemical Society, 121, 800.

30. Boone, D.H., et al, 1974, J. Vac. Sci. Technol. 11, 641.

31. Goward, G.W., 1972, "Materials and Coatings for Turbine Hot-Section Components", Gas Turbine Materials Conference Proceedings, Washington, D.C., p.85-96.

32. Felten, E.J., et al, 1974, "Coatings for Directional Eutectics", NASA CR-134735.

33. Rairden, J.R. and Jackson, M.R., 1976, "Coatings for Directional Eutectics", NASA CR-135050.

34. Levine, S.R., 1977, "Reaction Diffusion in the Nickel-Chromium-Aluminum and Cobalt-Chromium-Aluminum Systems", NASA TN D-8383.

35. Gedwill, M.A., 1971, "Cyclic Oxidation Resistance of Clad IN-100 at 1040^{o} and 1090^{o}C: Time, Cycle Frequency, and Clad Thickness Effects", NASA TN D-6276.

36. Gedwill, M.A., 1972, "Cyclic Furnace Oxidation of Clad WI-52 Systems at 1040° and 1090°C", NASA TN D-6730.

37. Freche, J.C. and Ault, G.M., 1976, "Progress in Advanced High Temperature Materials Technology", NASA TM X-71901.

38. Levine, S.R. and Clark, J.S., 1977, "Thermal Barrier Coatings - A Near Term, High Payoff Technology", NASA TM X-73586.

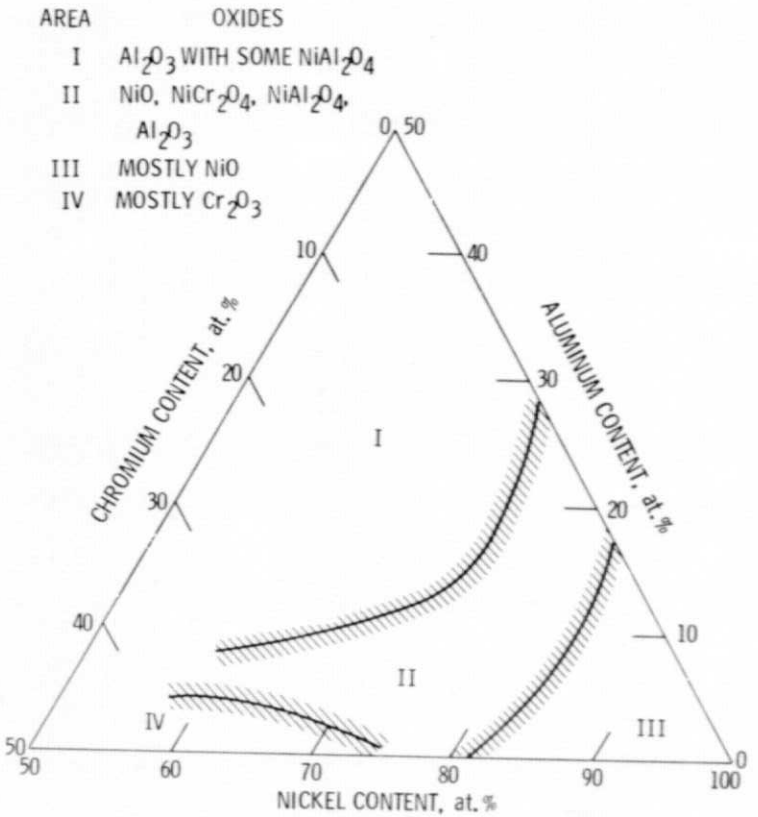

Figure 1. - Oxide map of cyclic oxidation in Ni-Cr-Al system at 1100° and 1200° C (6).

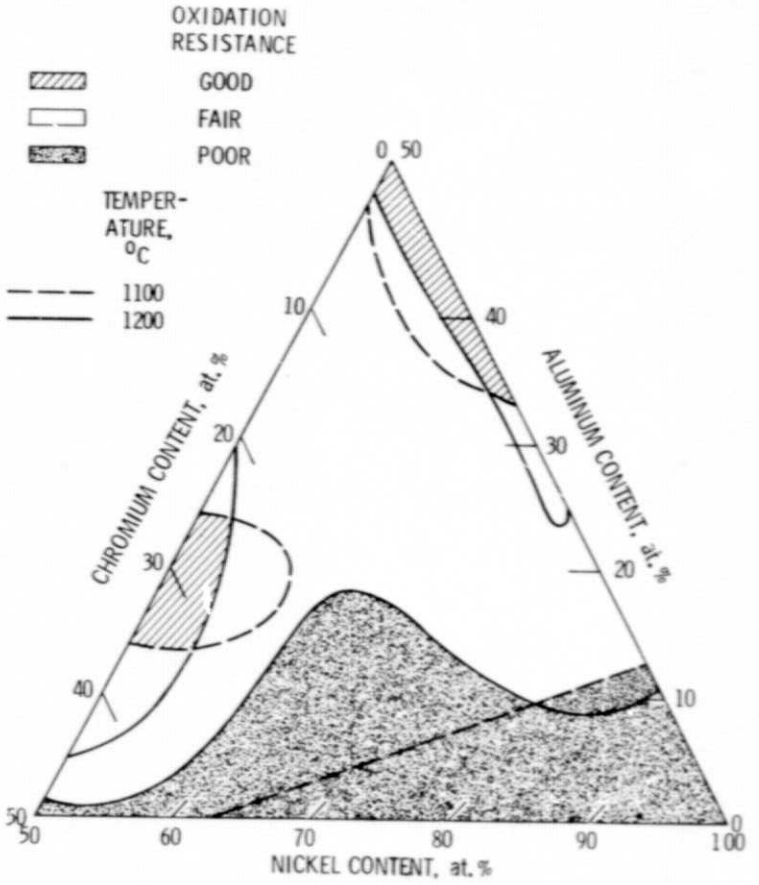

Figure 2. - Overall cyclic oxidation resistance for Ni-Cr-Al alloys at 1100° and 1200° C in still air (5).

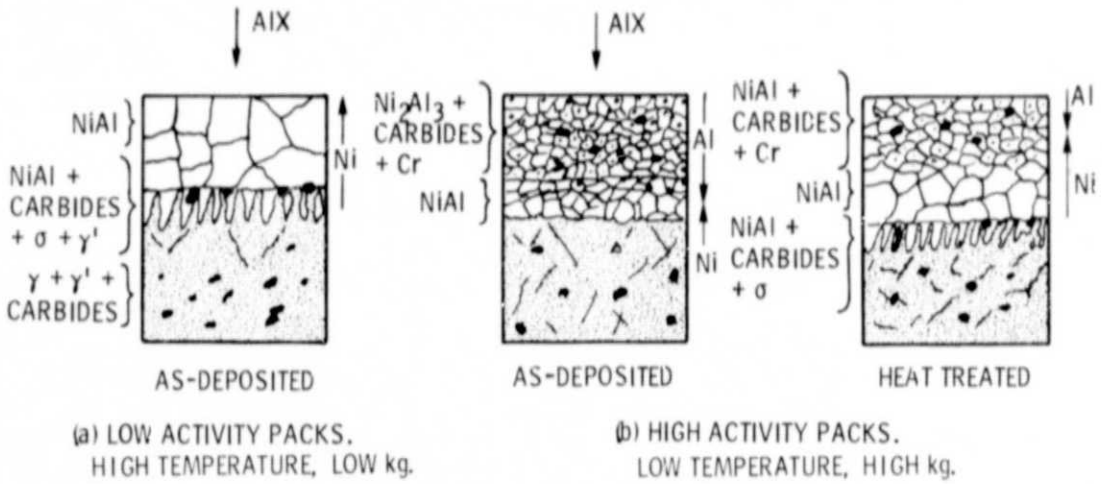

Figure 3. - Schematic representation of microstructure, constitution and formation mechanism of aluminide coatings.

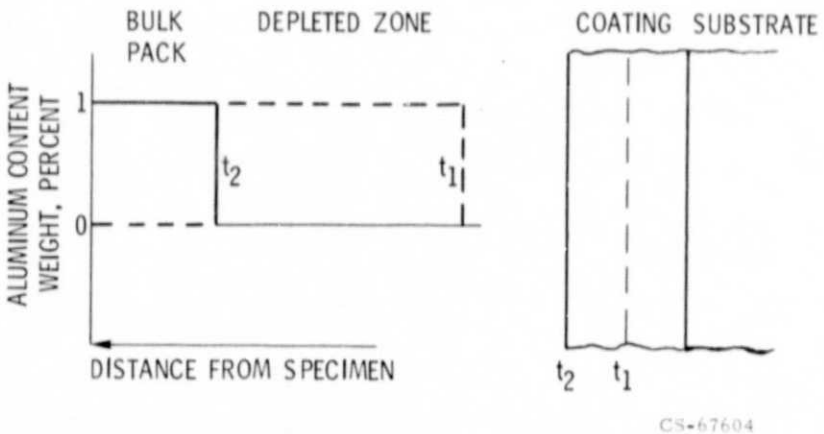

Figure 4. - Idealized depleted zone formation during pack aluminiding. Time, $t_2 > t_1$ (17)

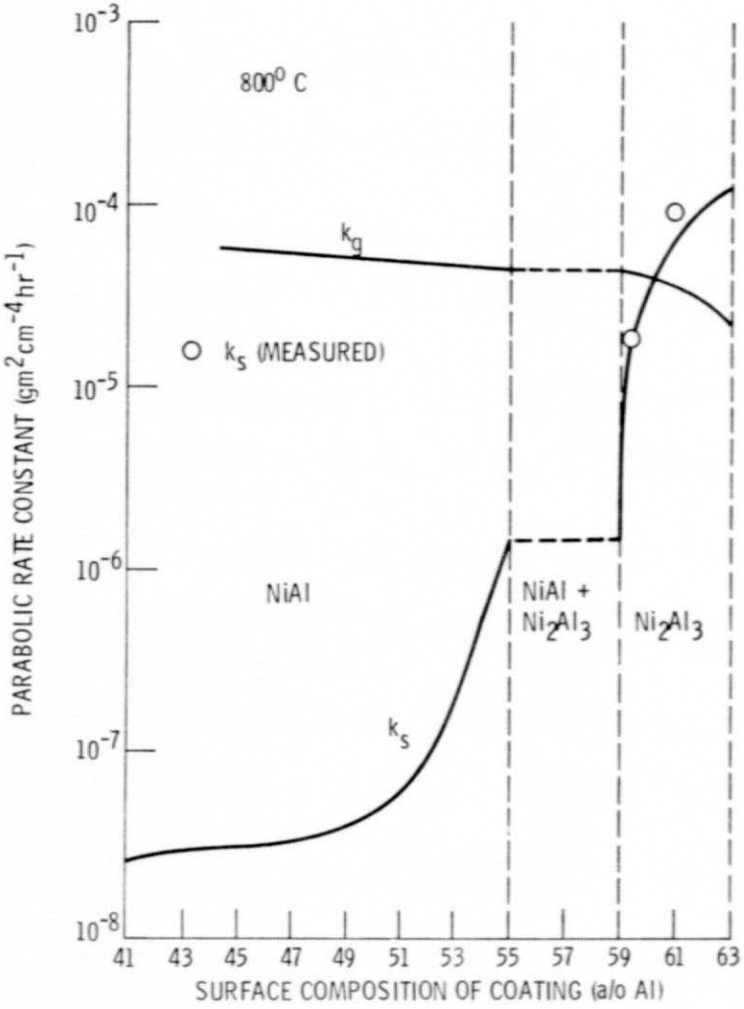

Figure 5. - Variation of rate constant in gas and solid phases with surface composition of coating at 800° C (20).

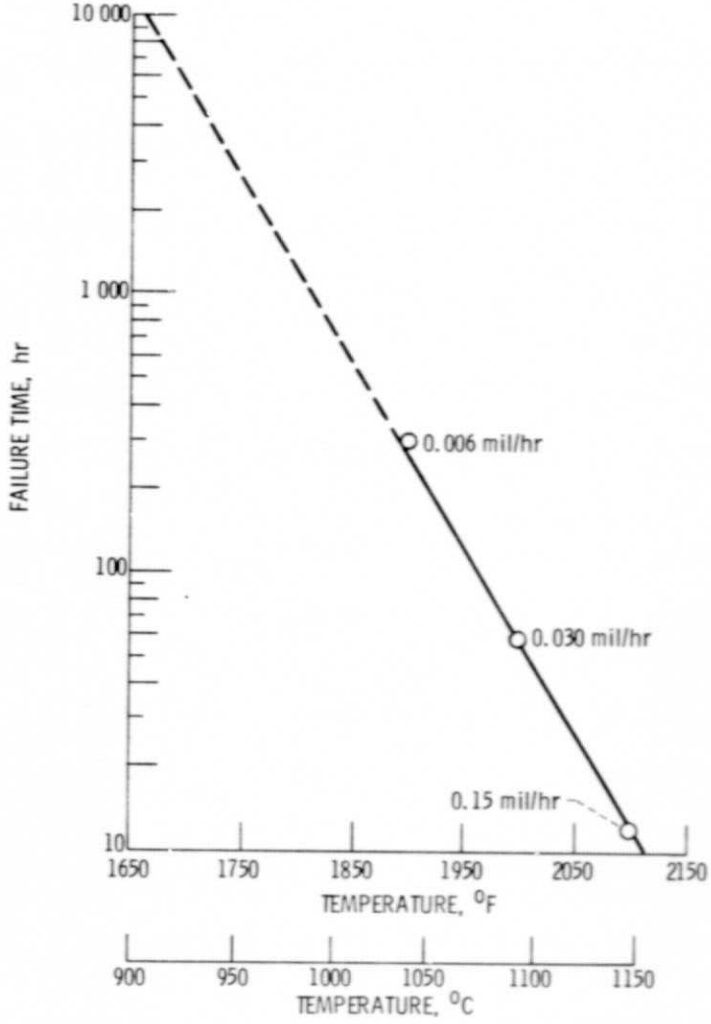

Figure 6. - Effect of temperature on life of aluminide coated WI-52 in high-velocity tests using 1-hour cycles (25).

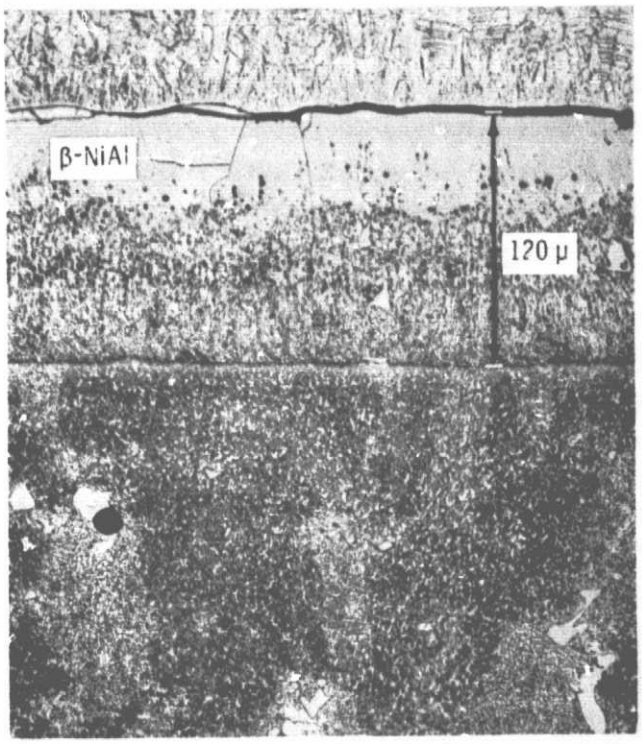

Figure 7. - As-coated Mar-M 200; X250 (29).

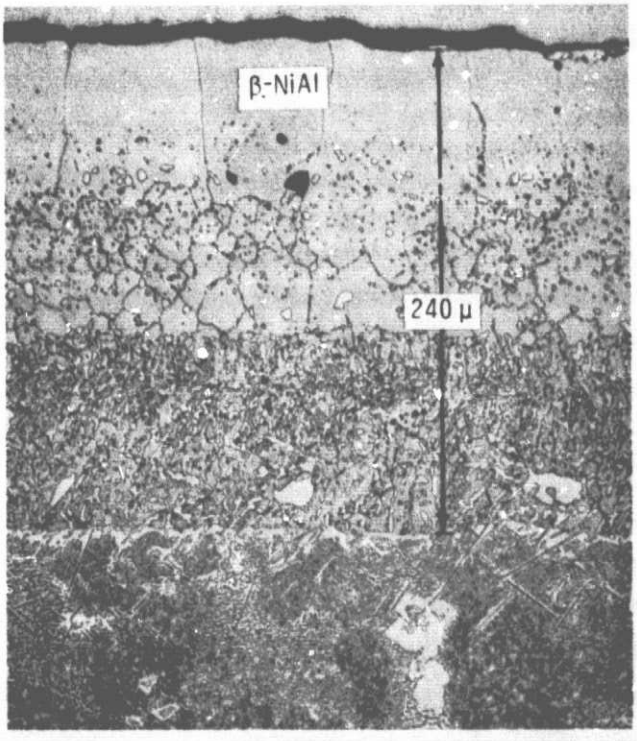

Figure 8. - Effect of diffusion annealing for 300 hours at 1100° C on coating structure of aluminized Mar-M 200; X250 (29).

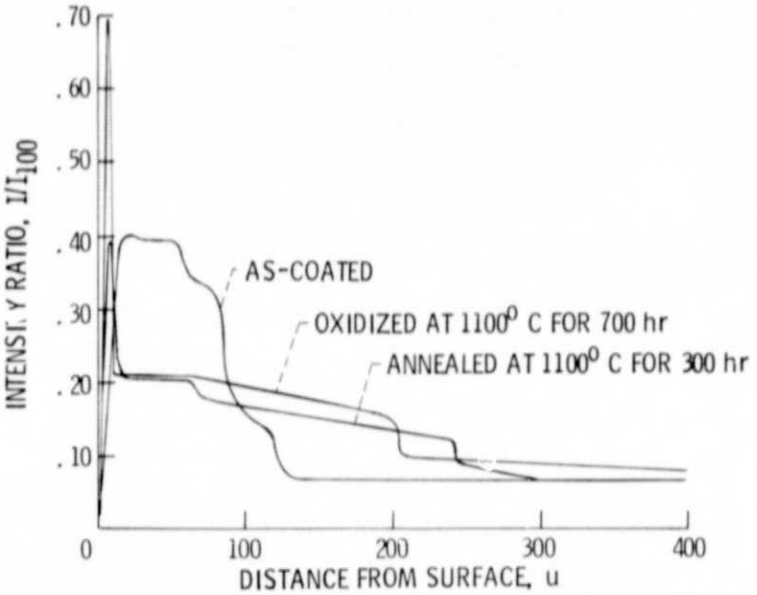

Figure 9. - Aluminum microprobe profiles for pack aluminized MAR M-200 (29).

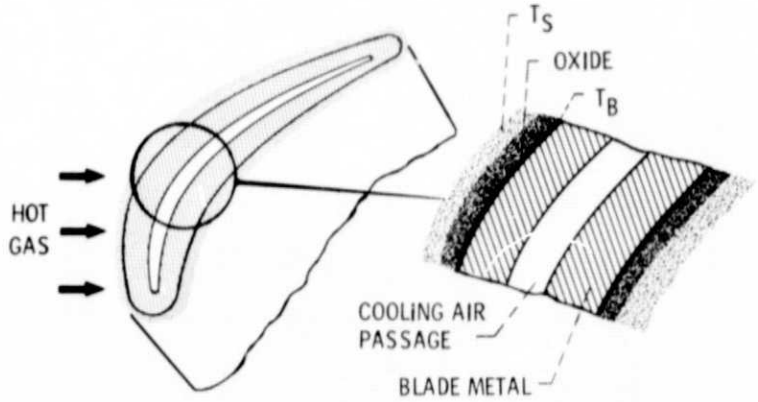

M 0.3 RIG - 182, 1-HR CYCLES

T_S = 1425° C (2600° F) T_B = 925° C (1700° F) ΔT = 480° C (900° F)

J 75 ENGINE TEST - 500, 1-MIN (AT MAX TEMP) CYCLES

T_S = 1060° C (1950° F) T_B = 900° C (1650° F) ΔT = 150° C (300° F)

Figure 10. - Thermal barrier concept - coatings insulate turbine blades (35).

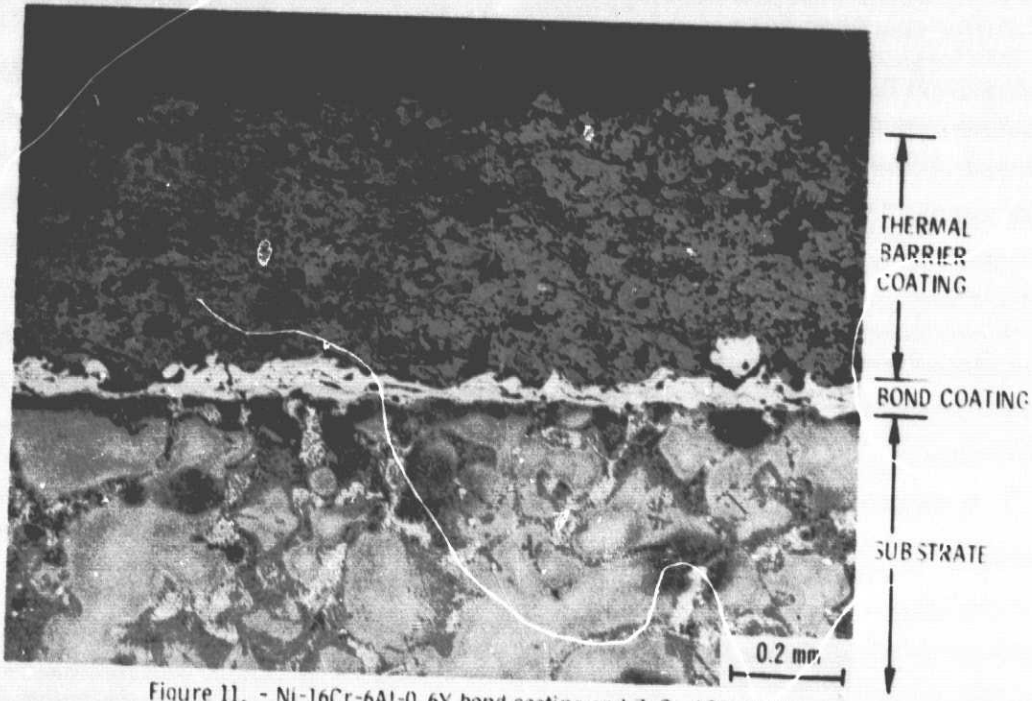

Figure 11. - Ni-16Cr-6Al-0.6Y bond coating and ZrO_2-12Y_2O_3 thermal barrier coating as deposited on DS Mar-M 200.